# A NUMERICAL INVESTIGATION INTO ELECTROOSMOTIC FLOW IN MICROCHANNELS WITH COMPLEX WAVY SURFACES

by

***Her-Terng YAU*** [a*], ***Cheng-Chi WANG*** [b], ***Ching-Chang CHO*** [c], ***and Cha'o-Kuang CHEN*** [c]

[a] Department of Electrical Engineering, National Chin-Yi University of Technology, Taichung, Taiwan
[b] Department of Mechanical Engineering, Far East University, Hsin-Shih, Tainan, Taiwan
[c] Department of Mechanical Engineering, National Cheng-Kung University, Tainan, Taiwan

Original scientific paper
UDC: 544.725.7:537.868:519.254
DOI: 10.2298/TSCI11S1087Y

*This study investigates the flow characteristics of electroosmotic flow in a microchannel with complex wavy surfaces. A general method of coordinate transformation is used to solve the governing equations describing the electroosmotic flow in the microchannel. Numerical simulations are performed to analyze the effects of wave amplitude on the electrical field, flow streamlines, and flow fields in the microchannel. The simulation results show that, compared to a traditional pressure-driven flow, flow recirculation is not developed in the electroosmotic flow in a microchannel with complex wavy surfaces. The simulations also show that the electrical field and velocity profiles change along the channel in the region of wavy surfaces. Non-flat velocity profiles are observed in different cross-sections of the channel in the region of wavy surfaces.*

Key words: *electroosmotic flow, microchannel, wavy channel, numerical simulation*

## Introduction

Recent years have witnessed significant advances in the microfluidic fields and have seen the development of many lab-on-a-chips (LOCs) for application in a diverse range of fields, including biological and chemical analysis, drug delivery, DNA hybridization, and so on. In modern microfluidic systems, most sample flows are manipulated using electrokinetically-induced driving forces. The resulting electroosmotic flow (EOF) can be easily controlled by adjusting the intensity of the electrical field applied at various points in the microfluidic device. Importantly, the velocity profile of an EOF, in a microchannel with a constant cross-section area, is a plug-like form, which is different from the parabolic velocity profile in a pressure-driven flow (PDF). As micro-electro-mechanical-systems (MEMS) technology continues to advance, EOF is emerging as a powerful alternative to conventional PDFs for microfluidic applications requiring a precise control of minute volumes of sample fluids. Therefore, fundamental understanding of fluid flow on electroosmotic flows is important to the operation of microfluidic devices.

* Corresponding author; e-mail: pan1012@ms52.hinet.net

In recent years, many researchers have proposed theory models and simulation techniques to investigate the EOF phenomena in microfluidic fields. For example, Arulanandam *et al.* [1] developed a theory model to simulate the flow characteristics of EOF in rectangular microchannels, and Patankar *et al.* [2] developed a 3-D numerical scheme to simulate EOFs in microchannels. Utilizing similar theory models, many researchers further study flow characteristics and associated transport properties in microchannels with irregular cross-sectional geometry. Hu *et al*. [3, 4] studied the EOF in microchannels with rectangular prismatic elements. It was shown that the average electroosmotic velocity in microchannels with rectangular prismatic elements was lower than that in a smooth microchannel. Wang *et al*. [5] and Wang *et al*. [6] utilize rectangular blocks mounted in microchannels to simulate the roughness of channel surfaces and to enhance the mixing effect on EOFs using the Lattice Poisson-Boltzmann Method and the Lattice Boltzmann Method, respectively. Chen *et al.* [7, 8] investigated the mixing characteristics of EOF and PDF in microchannels with simple wavy surfaces. The results have shown that the mixing performance on EOF and PDF was enhanced by increasing the wave amplitude or the length of the wavy section in the microchannel. Yang *et al.* [9] simulated the flow characteristics on EOF in a microchannel with sinusoidal surface roughness. Results showed that the bulk flow velocity was decreased when the roughness height was increased. Xiz *et al*. [10] studied the flow behaviors in a microchannel with a sinusoidal wall. Their results showed that flow recirculations were observed when a pressure gradient of sufficient strength in the opposite direction was added to an EOF in a wavy channel.

The current study performs numerical simulations to analyze the flow characteristics of 2-D, steady-state EOF in microchannels with complex-wavy surfaces. The flow behaviors on EOF in the microchannel with complex-wavy surfaces are compared with those observed in convectional pressure-driven flow. The simulations focus specifically on the effect of the wave amplitude on the flow field, flow streamlines, and electric field in the microchannel with complex wavy surfaces.

## Mathematical formulation

### *Governing equations*

In order to simplify the governing equations in this study, the flow field is assumed to be 2-D, incompressible and steady. The working fluid was assumed to be Newtonian liquid with constant fluid properties, and the gravitational and buoyancy effects are negligible. The governing equations used to describe the EOF are introduced in the section below. In a microchannel filled with an aqueous solution, the application of an external electric field induces an electrokinetic body force near the wall surface which affects the characteristics of the fluid flow. Therefore, the Navier-Stokes equations must be modified to the form:

$$\nabla \cdot \vec{V} = 0 \tag{1}$$

$$\rho\left[\frac{\partial \vec{V}}{\partial t} + (\vec{V}\cdot\nabla)\vec{V}\right] = -\nabla P + \mu\nabla^2\vec{V} + \vec{F}_E \tag{2}$$

where $\vec{V}$ is the velocity vector with components $u$ and $v$ in the x- and y-directions, respectively, $\rho$ – the fluid density, $t$ – the time, $P$ – the pressure, $\mu$ – the fluid viscosity, $\vec{F}_E$ = = $\rho_e E$ – the electrokinetic body force, $\rho_e$ – the net charge density, and $E$ is electric field.

In the present study, it is assumed that the EDL thickness is significantly smaller than the characteristic scale of the microchannel, and thus the flow characteristics within the EDL were modeled simply using Helmholtz-Smoluchowski velocity [11]. As a result, it is unnecessary to resolve the potential distribution within the EDL, and thus the computational complexity of the solution procedure is significantly reduced. The Helmholtz-Smoluchowski velocity can be modeled as [11]:

$$\vec{V}_{eo} = \mu_{eo} E \tag{3}$$

where $\mu_{eo} = -\varepsilon\varepsilon_0\zeta/\mu$ is the electroosmotic mobility, $\varepsilon$ is the dielectric constant of the solution, $\varepsilon_0$ – the permittivity of a vacuum, and $\zeta$ – the zeta potential. Note that the electrokinetic body force term ( $\vec{F}_E$ ) in eq. (2) can be neglected due to the assumption of a very thin EDL and the use of the Helmholtz-Smoluchowski velocity. The distribution of the electric potential in the microchannel is described by the following Laplace equation:

$$\nabla \cdot (\sigma \nabla \phi) = 0 \tag{4}$$

where $\phi$ is the electric potential and $\sigma$ is the electrical conductivity. Note that the electric field is equivalent to $E = -\nabla\phi$.

*Non-dimensionalization process*

The governing equations given in eqs. (1), (2) and (4) can be non-dimensionalized using the following non-dimensional parameters:

$$t^* = \frac{t}{L_c / V_r}, \nabla^* = L_c \nabla, \ \vec{V}^* = \frac{\vec{V}}{V_r}, P^* = \frac{P - P_r}{\rho V_r^2}, \varphi^* = \frac{ze}{k_b T}\varphi \tag{5}$$

Where $L_c$ is the characteristic scale of the microchannel, $V_r$ – the reference velocity, $P_r$ – the reference pressure, $z$ – the ionic valence, $e$ – the elementary charge, $k_b$ – the Boltzmann constant, and $T$ – the absolute temperature, and superscript * denotes a non-dimensional quantity. Note that the reference velocity is taken as $V_r = V_{eo}$.

Applying the non-dimensional quantities, the governing equations can be rewritten as:

$$\nabla^* \cdot \vec{V}^* = 0 \tag{6}$$

$$\left[ \frac{\partial \vec{V}^*}{\partial t^*} + (\vec{V}^* \cdot \nabla^*)\vec{V}^* \right] = -\nabla^* P^* + \frac{1}{\mathrm{Re}} \nabla^{*2} \vec{V}^* \tag{7}$$

$$\nabla^{*2} \phi^* = 0 \tag{8}$$

where Re is Reynolds number and is defined as $\mathrm{Re} = (\rho V_r L_c)/\mu$.

*Boundary conditions*

In this study, because the geometry structure presented in fig. 1 is symmetric, the computational domain is defined from a low surface to the center of the channel. In establishing the boundary conditions of the electrical potential for the simulation model shown in fig. 1, it is assumed that a constant electrical potential is applied to the inlet of the

channel, a reference electrical potential (*i. e.* grounding) is applied to the outlet of the channel, and an insulation condition is imposed on all wall surfaces. In setting the boundary conditions for the flow field, a fixed atmospheric value is applied to pressure in the inlet and outlet of the channel, a symmetric boundary condition is applied at the symmetric axis of the channel, and a slip condition is imposed on all wall surfaces.

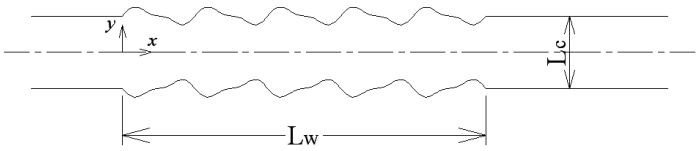


**Figure 1. Physical model**

*Geometry structure and numerical method*

In the simulations, the non-dimensional profile of the wavy-wall is modeled using the expression:

$$y^*(x^*) = \pm 0.5 \pm [\alpha_1 \sin(2\pi x^*) + \alpha_2 \sin(4\pi x^*)] \tag{9}$$

where $\alpha_1$ and $\alpha_2$ are wave amplitudes. Note that in the study, the ratio of the wave amplitudes is set as $\alpha_1$:$\alpha_2$ 2.5:1. The wavy form generated by eq. (9) is shown in fig. 1. A body-fitted grid system used to model the wavy-wall configuration is generated by solving a Poisson eq. [12].

Because the geometry configuration in wavy surface region is a non-orthogonal system, when simulating the fluid flow in the microchannel with complex wavy surfaces, as shown in fig. 1, the governing equations given in eqs. (6)-(8) are transformed from their original Cartesian coordinate system to a general curvilinear coordinate system. These transferred governing equations, in a general form, can be written as:

$$\frac{\partial}{\partial\xi}(\rho_\varphi U f) + \frac{\partial}{\partial\eta}(\rho_\varphi V f) = \frac{\partial}{\partial\xi}\left[\frac{\Gamma}{J}\left(\alpha\frac{\partial f}{\partial\xi} - \beta\frac{\partial f}{\partial\eta}\right)\right] + \frac{\partial}{\partial\eta}\left[\frac{\Gamma}{J}\left(-\beta\frac{\partial f}{\partial\xi} + \gamma\frac{\partial f}{\partial\eta}\right)\right] + JS \tag{10}$$

where $f$ is a generalized variable; $\xi$ and $\eta$ are the axes of the transformed coordinates, respectively; $U = (y_\eta u - x_\eta v)$ and $V = (x_\xi v - y_\xi u)$ are the velocities of the transformed co-ordinates; $S$ is source term included the pressure gradient term and transient term; $\alpha = (x_\eta^2 + y_\eta^2)$, b = $(x_\xi x_\eta + y_\xi t_\eta)$ and $\gamma = (x_\xi^2 + y_\xi^2)$ are the parameters of the transformed coordinates, respectively; and $J = x_\xi y_\eta - x_\eta y_\xi$ is the Jacobian factor.

These transferred governing equations and corresponding boundary conditions were solved using the finite-volume numerical method [13]. A second-order scheme is used to discrete the convection terms. The velocity and pressure fields were coupled using the SIMPLE algorithm [13]. The discreted algebraic equations were solved using the TDMA (tri-diagonal matrix algorithm) scheme. Note that prior to the simulations, a grid-sensitivity analysis was performed to establish a suitable mesh size for satisfying the numerical accuracy.

## Results and discussion

A series of numerical simulations was performed to investigate the characteristics of 2-D, steady-state EOF in microchannels with complex-wavy surfaces shown in fig. 1. In the simulations, it is assumed that the zeta potential on all wall surfaces is uniform, the intensity

of the externally-applied electric field is given as $E$ = 20 V/cm, and the Reynolds number is specified as $\mathrm{Re} = 0.1$.

Figure 2 plots the distribution of the electrical potential in the microchannel with complex wavy surfaces. It can be seen that the equi-potential lines are distorted as electrical potentials pass through the region of the wavy surface. A sparser equi-potential line is observed near the wave trough, and a denser equi-potential line is observed near the wave crest. The trend of distribution on the electrical potential is more evident as the wave amplitude increases.

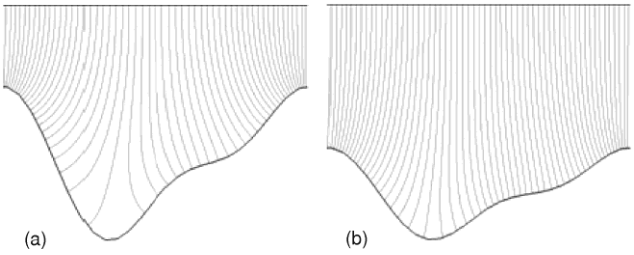


**Figure 2. Distribution of electrical potential in the microchannel when the wave amplitude is (a) $\alpha_1$ = 0.2, and (b) $\alpha_1$ = 0.1**

Figure 3 further illustrates the strength of the electrical field along the wall surface. As described above, the strength of the electric field is greater near the wave crest and is weaker near the wave trough. The variation range of the electrical field strength increases when the wave amplitude is increased. In addition, it can be seen that the variation of the electrical field strength along the wavy surface is asymmetric because of the effect of the geometric configuration. The distribution of the electrical field affects the flow characteristics in the microchannel.

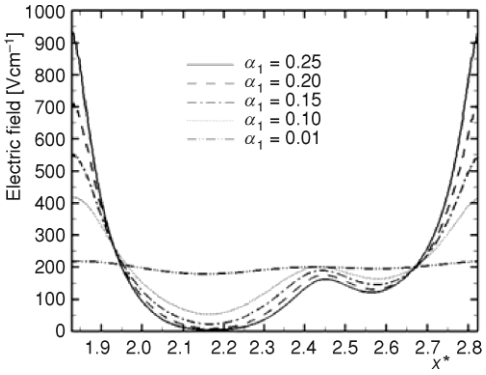


**Figure 3. Electric field on the wall surface along the microchannel**

Figure 4 illustrates the flow streamlines and velocity vectors for EOF within the micro-channel with complex wavy surfaces. In EOF, an electro-kinetic driving force is induced as a result of the interaction between the EDL potential and the externally-electric field. The driving force acts only on the fluid near the walls of the microchannel. The bulk fluid is dragged into motion via a momentum coupling effect, with the driven fluid near the microchannel walls. Therefore, it can be seen that the flow streamlines follow the profile of the wavy surface in the EOF. Furthermore, it is evident that no flow recirculations are formed in the trough regions between neighboring wave structures. The EOF behavior is quite different from that observed in PDF.

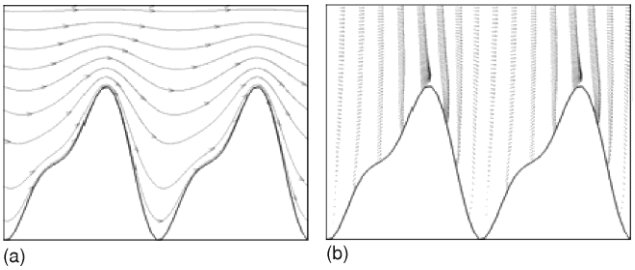


**Figure 4. (a) Flow streamlines, (b) Velocity vectors in electroosmotic flow**

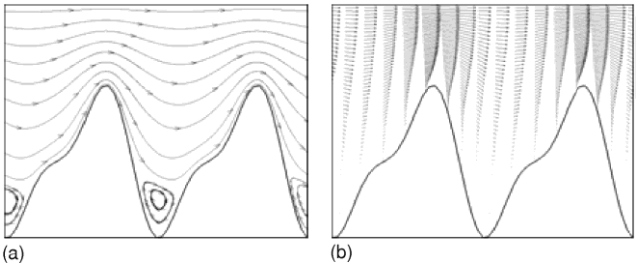


**Figure 5. (a) Flow streamlines, (b) Velocity vectors in pressure-drivem flow**

Figure 5 illustrates the flow streamlines and velocity vectors within the microchannel with complex wavy surfaces for PDF. Note that in the PDF, the electrokinetic effect was not considered. In other words, the Navier-Stokes equations, without body force terms, are used to simulate the flow behaviors on the PDF. In addition, in the set of boundary conditions in the PDF, a constant velocity value is imposed at the inlet of the channel, a fully developed condition is imposed at the outlet of the channel, and a no-slip condition is used on all wall surfaces. Note that for the reference velocity in the PDF, the mean velocity of the channel is taken. In the PDF, an external force is applied to overcome the frictional force near the wall surfaces induced by viscous effects. When the wave amplitude is large enough, the interaction of the momentum with viscous effects induces flow recirculation in the vicinity of the wave trough, in order to satisfy the principles of mass conservation. Furthermore, it can be seen that the flow recirculation is asymmetric because the wavy form is complex. Comparing the EOF with the PDF, the forms of the velocity vectors in the microchannel are quite different because the driving manner on the fluid is quite different.

In order to further compare velocity distributions for the EOF with PDF within the microchannel with complex wavy surfaces, fig. 6 illustrates the u-velocity profiles at different cross-section locations in the channels. In general, in the EOF, the magnitude of the induced electroosmotic velocity is proportional to the strength of the electrical field near the wall surface. It can be expected that the distribution of the induced electroosmotic velocity, near the wavy surface along the channel, has the same trend as fig. 3. In the wave trough, the strength of the electrical field is weaker because of the effect of the geometrical structure. Therefore, it can be seen that the induced electroosmotic velocity on the wave trough is also weaker. In the same cross-section away from the wall surface, the velocity is larger than that near the wall surface because of the effect of the inertia force, as shown in figs. 6(a) and (d). In addition, it is evident that no reverse velocity is formed in this cross-section as the wave amplitude is increased. In PDF, when the wave amplitude is smaller, the interaction between momentum and viscous effects cannot generate an opposite velocity in the region of the wave trough. Therefore, flow recirculation is not induced. When the wave amplitude is large enough, an opposite velocity induced by the interaction between momentum and viscous effects is generated near the wave trough in order to satisfy the principle of mass conservation. Hence, flow recirculation phenomena are observed. Comparing the EOF with the PDF, it is clear that flow behaviors are quite different in the microchannel with complex wavy walls.

As the width of the channel is gradually decreased, the electrical field strength is gradually increased near the wall surfaces because of the geometrical effect. Therefore, the induced electroosmotic velocity near the wall surfaces is also gradually increased. Hence, in the cross-section of the center of the wavy surface, a larger electroosmotic velocity than that in the trough is induced near the wall surface. In the same cross-section, away from the wall surface, because of the effect of the inertia force, the velocity profile is slightly distorted in

order to satisfy the principle of mass conservation, as shown in figs. 6(b) and (e). For the PDF, in the same cross-section, it can be seen that a slightly distorted parabolic velocity profile is observed as a result of the change in the inertia effect caused by the variation in the channel width.

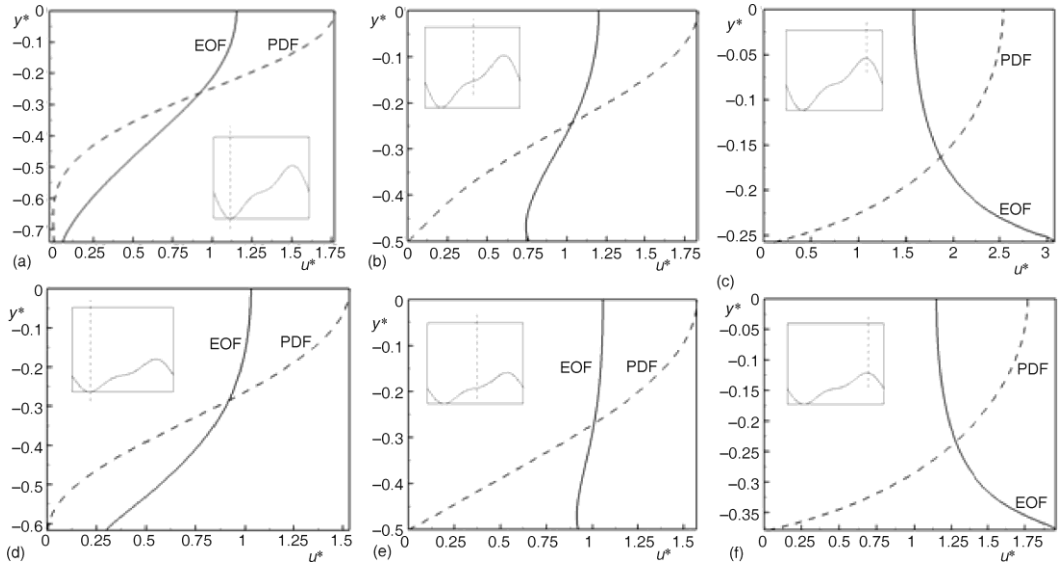


**Figure 6. u-velocity profiles at different cross-section location of microchannel. Note that the wave amplitude is $\alpha_1$ = 0.2 in (a)-(c), and the wave amplitude is $\alpha_1$ = 0.1 in (d)-(f)**

In the cross-section on the wave crest, because the largest electrical field strength is observed, the largest electroosmotic velocity near the surface is obtained. In order to satisfy the principle of mass conservation, a concave velocity profile is observed in this cross-section, as shown in figs, 6(c) and (f). In PDF, because of the smallest width of channel in the cross-section, the largest velocity is obtained at the center of the channel in order to satisfy the principle of mass conservation. These flow phenomena described above are more evident when the wave amplitude is increased. Comparing the EOF with the PDF at the same cross-section of the channel, it is observed that the variation range of velocity on EOF is smaller than that on PDF. In other words, the EOF velocity profiles are flatter than those generated in PDF.

The above indicate results from fluid motion into an EOF in a microchannel with complex wavy surfaces. The results can be used to explain fluid behavior in microchannels with surface roughness in order to accurately operate the fluid, or can be utilized to design microfluidic devices (*e. g.* an enhancement in fluid mixing by complex wavy surfaces) and so on.

## Conclusions

The present study conducted a numerical investigation into the characteristics of 2-D, steady-state electroosmotic flow in a microchannel with complex wavy surfaces. The effect of wave amplitude on the flow field, flow streamlines, and electrical field were investigated. The results from the electroosmotic flow were compared with traditional pressure-driven flow. The

simulation results indicate that no flow recirculation is observed on the electroosmotic flow in a microchannel with complex wavy surfaces. The electroosmotic flow characteristics differ significantly from those observed in pressure-driven flow. In addition, the strength of the electrical field changes along the wall surface, as a result creating a variation in the channel wall. The results affect the velocity distribution on the electroosmotic flow within the microchannel. A non-flat velocity distribution is observed in different cross-sections of the channel in the region of the wavy surface. Based on the flow motion into an electroosmotic flow in microchannels with complex wavy surfaces, more accurate flow operation in microfluidic systems can be achieved.

## Acknowledgment

The authors gratefully acknowledge the financial support provided to this study by the National Science Council of Taiwan under Grant No. NSC-98-2221-E-167-030-MY2.

## References

[1] Arulanandam, S., Li, D., Liquid Transport in Rectangular Microchannels by Electroosmotic Pumping, *Colloids and Surfaces A: Physicochemical and Engineering Aspects*, *161* (2000), 1, pp. 89-102
[2] Patankar, N. A., Hu, H. H., Numerical Simulation of Electroosmotic Flow, *Analytical Chemistry, 70* (1998), 9, pp. 1870-1881
[3] Hu, Y., Werner, C., Li, D., Electrokinetic Transport Through Rough Microchannels, *Analytical Chemistry, 75* (2003), 21, pp. 5747-5758
[4] Hu, Y., Xuan, X., Werner, C., Li, D., Electroosmotic Flow in Microchannels with Prismatic Elements, *Microfluidics and Nanofluidics, 3* (2007), 2, pp. 151-160
[5] Wang, M., Wang, J., Chen, S., Roughness and Cavitations Effects on Electroosmotic Flows in Rough Microchannels Using the Lattice Poisson-Boltzmann Methods, *Journal of Computational Physics, 226* (2007), 1, pp. 836-851
[6] Wang, D., Summers, J. L., Gaskell, P. H., Modelling of Electrokinetically Driven Mixing Flow in Microchannels with Patterned Blocks, *Computers and Mathematics with Applications, 55* (2008), 7, pp. 1601-1610
[7] Chen, C. K., Cho, C. C., Electrokinetically-Driven Flow Mixing in Microchannels with Wavy Surface, *Journal of Colloid and Interface Science, 312* (2007), 2, pp. 470-480
[8] Chen, C. K., Cho, C. C. A Combined Active/Passive Scheme for Enhancing the Mixing Efficiency of Microfluidic Devices, *Chemical Engineering Science, 63* (2008), 12, pp. 3081-3087
[9] Yang, D., Liu, Y., Numerical Simulation of Electroosmotic Flow in Microchannels with Sinusoidal Roughness, *Colloids and Surfaces A: Physicochemical and Engineering Aspects, 328* (2008), 1-3, pp. 28-33
[10] Xia, Z., *et al*., Electroosmotically Driven Creeping Flows in a Wavy Microchannel, *Microfluidics and Nanofluidics, 6* (2009), 1, pp. 37-52
[11] Probstein, R. F., Physicochemical Hydrodynamics an Introduction, John Wiley & Sons, New York, 1994
[12] Thomas, P. D., Middlecoff, J. F., Direct Control of the Grid Point Distribution in Meshes Generated by Elliptic Equations, *AIAA Journal, 18* (1980), 6, pp. 652-656
[13] Patankar S.V., Numerical Heat Transfer and Fluid Flow, McGraw-Hill, New York, 1980

Paper submitted: June 28, 2010
Paper revised: July 30, 2010
Paper accepted: November 11, 2010